Transactions of the 15th International Conference on
Structural Mechanics in Reactor Technology (SMiRT-15)
Seoul, Korea, August 15-20, 1999

Ultimate Capacity Analysis of 1/4 PCCV Model Subjected to Internal Pressure

Kenji Yonezawa[1], Masahito Akimoto[1], Katsuyoshi Imoto[1] and Yukio Watanabe[2]

1) Obayashi Corporation, Japan
2) The Japan Atomic Power Company, Japan

ABSTRACT

As presented in the papers of the SMiRT-14 [1] [2], the ultimate capacity pressure tests of a 1/4 scale prestressed concrete containment vessel (PCCV) model will be held in year 2000. Authors have conducted a preliminary analytical investigation to predict the nonlinear behavior up to ultimate capacity and to estimate approximate potential failure mode.

The target of this project is not only to predict nonlinear behavior of the 1/4 PCCV model, but also to establish a reliable evaluation method of actual PCCVs subjected to internal pressure.

This paper describes modeling methods and results by two global analyses:

1) Modification of friction effect between concrete and unbonded tendons which takes an important role in determining force distributions in tendons, specially curved ones.
2) Results by global analyses with 3D-shell 360° model and axi-symmetric model.

1. INTRODUCTION

The 1/4 scale PCCV model contains 90 vertical and 108 horizontal tendons for prestressing. Therefore, the nonlinear behavior of the PCCV is strongly influenced by the tendon behavior. In general, curved unbonded tendons have friction effect and this effect should be considered to evaluate the force distribution of tendons in the analyses.

At first, the modification of the friction effect between concrete and unbonded tendon is investigated. Carrying out some numerical experiments, an appropriate tendon friction model is proposed and this will be applied for the global and local analyses.

Secondly, the global analyses with axisymmetric model and 3D-shell 360° model which considers above friction model are performed. The 3D-shell 360° model takes into account all the non-axisymmetry, such as tendon layout in the dome, buttresses, equipment hatch (E/H), personnel airlock (A/L) and local concentration of rebar arrangement around the small penetrations for main steam (M/S) and feed water (F/W).

Finally, the influence of penetrations and rebar arrangement on global behavior and the potential failure patterns are discussed by use of the analytical results.

Computer code used here is FINAL[3] which have been developed by Obayashi corporation.

2 TENDON FRICTION MODEL

2.1 FRICTION MODEL

Shear force is usually transmited by friction through contact surface between a prestressed

tendon and a reinforced concrete (RC) body, especially on curved surface. This kind of contact problem may often cause numerical instability in the computation of numerical analysis. Therefore, the tendon friction model which might be able to avoid the numerical instabilities, is examined at first.

The model is assumed to obey the classical Coulomb friction theory, i.e., the surfaces don't slide each other so long as the shear stress between a tendon and a RC body is less than μ (the friction coefficient) times the normal stress to the surface.

(a) Sliding surface and interface element

The friction model is represented by use of a linkage element which is composed of three springs being normal to each other, as shown in Fig.1;

in this figure,

$\vec{t}$ is the tangent vector to the slide line.

$\vec{n}_1$ is the 1st normal vector to the slide line in radial direction.

$\vec{n}_2$ is the 2nd normal vector to the slide line in normal to the other springs.

The tendon nodes are allowed to slide only in the direction of the tendon.

(b) Characteristics of the friction model

Where a tendon element is arranged on a curved RC body with double curvatures, the pressure stress vector is normal to the contact surface. For this case of tendon layout, a normal stress to contact surface is assumed to take the following stress ($\vec{\sigma}$) by use of two independent spring stresses ($\vec{\sigma}_1$, $\vec{\sigma}_2$) in the directions ($\vec{n}_1$,$\vec{n}_2$).

$$\vec{\sigma} = \sqrt{\vec{\sigma}_1^{\,2} + \vec{\sigma}_2^{\,2}}$$

The stress – displacement relationships are assumed to be bi-linear as shown in Fig.2. When the stress (τ) reaches the specified stress($\mu\vec{\sigma}$), sliding begins to start, and the second stiffness is assumed to be very small for further increments. The second stiffness should be 0, but small stiffness (hypothetical) must be considered to avoid numerical instabilities. The amount of this hypothetical stiffness depends on the problems to be analyzed.

For the two springs in the directions normal to sliding line, linear elastic is assumed.

2.2 ELEMENT VERIFICATION

(a) Numerical example I

Numerical experiments are carried out to obtain the proper stiffness (K2), and to confirm whether the friction model does work well. Fig.3 shows two examples.

Both models consist of a concrete body, horizontal tendons, and friction elements. The RC body is chosen to be semicircular representing a part of the PCCV's cylinder. The model I is loaded by pulling the tendons at one end and fixed at the other end.

Performing parametric computations, it is found that numerical instability can be avoided by setting to be K2=.K1/1000, but the numerical instability occurred when K2 is smaller than K1/1000.

Fig.4 shows comparison of the tendon force distributions obtained from analytical result and theoretical solution at three load levels, P_0 = 0.245 MN, 0.490 MN (elastic state), and 0.735 MN (plastic state). The theoretical equation is given as,

$$P(\theta) = P_0 \times e^{-\mu\theta}$$

Where μ is the friction coefficient (μ =0.21) [4], and P_0 is the tensile force of the tendon

at θ =0 (radian).

From this figure, some differences between the analytical result and the theoretical ones can be seen, but they seem to remain in allowable range up to the plastic state for actual use.

Fig.5 shows the strain distribution of the tendon along the arc of a concrete body. At P=0.735MN of the pulling load where tendon enters in plastic state, the gradient of strain distribution becomes very large at the portion near the pulling end, in comparison with that in elastic state.

(b) Numerical model II

Secondly, the applicability of the above friction model is investigated for the case that rebar ratio is not uniform in RC body subjected to increasing internal pressure, as shown in Fig.3. The rebar ratio of RC body in the range of $60^\circ < \theta < 120^\circ$ is lager than that of the rest.

Strain distributions of tendons are shown Fig.5 for the cases of two pressure levels where the state of tendon stress are in elastic and in plastic state. Both strain distributions indicate non-uniformity along the arc but symmetry to the axis at $\theta = 90^\circ$, because of the effects of friction and stiffness change of RC body in the circumferential direction.

As the results, the friction effects between unbonded tendon and RC body can be evaluated successively by the model examined.

3. GLOBAL ANALYSES OF 1/4PCCV MODEL

3.1 ANALYTICAL MODELING

Computational grids of two analyses are shown in Fig.6 and Fig.7.

1) Axisymmetric Model

As for axisymmetric analysis, a 3-D FEM for the narrow wedge of vertical section(2°) is used instead of using normal axisymmetric FEM . This model plane is chosen at the 135° azimuth, which is reasonably far from the penetrations.

The concrete is modeled with 8 nodes solid element. The meridional tendons are represented with truss elements and attached to the concrete with sliding elements. The bond characteristics between concrete and meridional tendons are assumed to be an unbonded. Reinforcement rebars are represented with truss elements and a shell layers which are given an area equivalent to the rebar area and Poisson's Ratio of zero to avoid any in-plane/out of plane stress - strain interactions. The liner is constructed of quadratic shell elements and liner anchors are represented with shell layer which are given an area equivalent to the liner anchor area. Perfect bond is assumed for the bond characteristics between rebar and concrete.

2) 3D-Shell 360° Model

3D-shell 360° model as shown in Fig.6, which idealized the whole 1/4 PCCV model, takes into account the non-symmetric tendon layout in the dome, buttresses, E/H, A/L and local concentration of rebar arrangement around these penetrations. The layout of meridional tendons is idealized accurately in this model as much as possible. As a boundary condition, the bottom of cylinder is assumed to be fixed by considering the results of axisymmetric analysis.

The reinforced concrete wall is modeled with quadratic multi-layered shell elements. The meridional and hoop tendons are represented with truss elements and attached to the concrete with sliding elements. As the friction characteristics between concrete and tendons, the friction model discussed above is adopted. The liner is constructed of quadratic shell elements.

3.2 MATERIAL MODEL

As for concrete model, authors adopted the equivalent uniaxial strain model which is proposed by Darwin et al. [5] and developed for tree-dimensional analysis by Murray [6]. The five-parameter model developed by Willam et al. [7] in the axisymmetric model, and Kupfer's model [8] in 3D-shell 360° model are used for failure surface. The five - parameters obtained from the experiments by Ohnuma et al are adopted. [9]. As for basic uniaxial stress -strain relationship, modified Ahmad model [10] is used in the compression zone, elastic behavior is assumed until cracking in the tension zone. After cracking, tension cut-off is assumed and stiffness normal to the crack plane is set to be zero. Al-Mahaidi equation [11] is used for shear retention model in cracked plane.

As for the steel materials, the elasto-plastic theory based on the von Mises yield criterion is used for nonlinear behavior. Stress-strain relationships of the steel materials are assumed to be multi-linear.

Material properties of concrete and steel used in the analyses are to be same as those given in [4].

3.3 ANALYTICAL RESULTS

The pressure - radial and vertical displacement relationships by both analyses are compared in Fig.8 and Fig.9, respectively.

The heights where the maximum radial displacements are obtained by both analyses are almost the same at about the mid-height (EL.7200) of the cylinder. The apex of the dome begins to move downward at pressure larger than 1.5MPa as shown in Fig.9. But this amount is fairly small in comparison with the radial displacement at the mid-height of the cylinder.

The displacement of 360° model becomes larger than that of axisymmetric model at pressures above 1.2MPa. The sequences of non-linearity by the two analyses are found to be almost the same, as those, firstly concrete cracking at pressure of 0.6MPa, liner yielding at 0.92MPa, rebars yielding at 0.93MPa, hoop tendons yielding around mid-height portion at 1.3Mpa, and finally reaching the ultimate capacity of Pmax=1.55Mpa.

A deformation mode and contour obtained by 360° model at Pmax are shown in Fig.10. And comparisons of the radial deformation modes of horizontal section (EL.7375) at the pressure of Pmax are shown in Fig.11.

By the 360° model, the location of the maximum displacement(467mm at Pmax) is found at general portion about 230° azimuth between the buttress and M/S. And it can be seen from Fig.10 that the deformation mode is not axisymmetric at all, due to the effects of penetrations (M/S, F/W, E/H, A/L), buttresses and non-symmetric tendon layout in the dome.

In Fig.11, the radial displacement of the 360° model appears to be larger as a whole than that of axisymmetric model. This is because all penetrations and local concentration of rebar arrangement are precisely modeled in the 360° model, but not in axisymmetric model. Therefore the axisymmetrical analysis is not appropriate to evaluate exactly the non-linear behavior of PCCV structures.

The contour of von Mises total strain in the liner at Pmax is shown in Fig.12. The strain concentrations of the liner occur at several portions, such as the rebar cut-off sections around the penetrations and buttress as shown in Fig.12.

The locations and amount of the maximum strain of materials (rebars, liner, tendons) are summarized corresponding to pressure levels in Table.1 and Fig.13. The thick lines and hatches in Fig.13 indicate the boundary lines of rebar cut-off sections where hoop rebar ratios change.

The maximum tendon strain is found to be in hoop tendon near buttress at EL8000, reaching

7.53% at Pmax. The maximum principle strain of liner is found at the hoop rebar cut-off sections around M/S, reaching 9.29% at Pmax. The maximum strain of rebar changes it's location according to the pressure levels. That is, the maximum strains are found at the hoop rebar cut-off section around A/L at 1.4MPa, at the hoop rebar cut-off section on azimuth 0° at 1.45MPa, and at the hoop rebar cut-off section around the buttress at Pmax, respectively.

In reference [4], the ultimate strains of materials are given for 1/4 PCCV, i.e. 6.3% for tendons, 33% for steel liner and about 22% for rebars. Comparing these data with the analytical results described above, there is a margin in the liner and rebars but the strain of tendons exceeds the ultimate strain. The hoop tendon breaking at EL.8000 may possibly occur at internal pressure of about 1.55MPa before the liner tearing and rebar breaking.

4. CONCLUSIONS

The conclusions obtained from this study are as follows,

1) By carrying out numerical experiments, the tendon friction model proposed here is confirmed to be able to avoid numerical instability up to the ultimate capacity, and to be effective for actual use.
2) The nonlinear behavior of PCCV under internal pressure is strongly influenced by the non-symmetries of the structure, such as penetrations (M/S, F/W, E/H, A/L), buttresses and non-symmetric tendon layout in the dome. Therefore the axisymmetrical analysis is not appropriate to evaluate exactly the non-linear behavior of PCCV structures.
3) The strain concentrations of the liner occur at the several portions near the rebar cut-off sections around the penetrations and buttresses.
4) The hoop tendon breaking at EL.8000 may possibly occur at the internal pressure of about 1.55MPa before the liner tearing and rebar breaking occur.
5) In order to predict the ultimate behavior of PCCVs more exactly, lots of local analyses with more fine mesh models as listed in Ref.[1] must be performed in addition to the global analyses here.

REFERENCES

[1] Dameron, R. A. et al.: Preliminary analysis of a 1/4 scale prestressed concrete containment vessel model, SMiRT 14, H03/3, pp.89-96. Aug., 1997.

[2] Hessheimer, M. F. et al.: Instrumentation and testing of a prestressed concrete containment vessel model, SMiRT 14, H03/4, pp.97-104. Aug., 1997.

[3] Takeda, T. et al.: Report on Tests of Nuclear Prestressed Concrete Containment Vessels, Concrete Shear in Earthquake, Edited by T. C. C. Hsu, S. T. Mau, Elsevier Applied Science, pp.163-172, 1992.

[4] Tsurumaki, S. et al.: Seismic Proving Test for Concrete Containment Vessels (I.PCCV) Part6-11, Annual Convention of AIJ, Proceeding of Structures II, pp.1079-1090, Sept., 1998, in Japanese.

[5] Darwin, D. et al.: Nonliner Biaxial Stress-Strain Law for Concrete, J. of EM Div., ASCE, Vol.103, No. EM2, pp.229-241, April, 1977.

[6] Elwi, A. A. et al.: A 3D Hypoelastic Concrete Constitutive Relationship, J. of EM Div., ASCE, Vol. 105, No.EM4, pp.623-641, Aug., 1979.

[7] Willam, K. J. et al.: Constitutive Model for the Triaxial Behavior of Concrete, Proc. of Int. Assoc. for Bridge & Stru. Eng., Vol.19, pp.1-30, 1975.

[8] Kupfer, H. B.: Behavior of Concrete under Biaxial Stress, J. of E. M. Div., ASCE, Vol.99, No.EM4, pp.853-866, Aug., 1973.

[9] Ohnuma, H. et al., Ultimate Strength Property of Concrete under Triaxial Compressive Stresses, Report of CRIEIPI, No.381021, Dec., 1981, in Japanese.

[10] Naganuma, K.: Stress-Strain Relationship for Concrete under Triaxial Compression, J. of Struc. & Const. Eng. (Transactions of AIJ), No.474, pp.163-170, Aug., 1995, in Japanese.

[11] Al-Mahaidi, R. S. H.: Nonlinear Finite Element Analysis of Reinforced Concrete Deep Members, Report 79-1, Dep. of Structural Engineering, Cornell Univ., Jan., 1979.

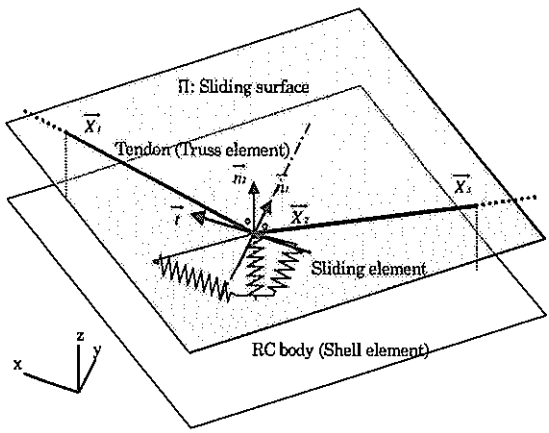

Fig. 1 Schematic view of sliding element

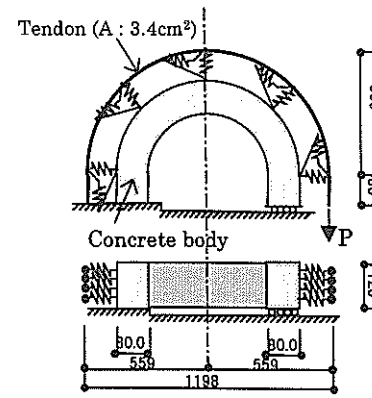

Numerical example I

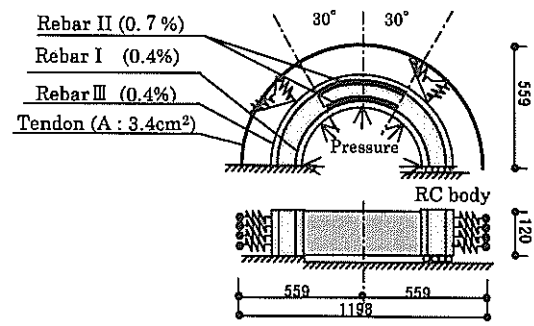

Numerical example II

Fig. 3 Numerical models (Unit : cm)

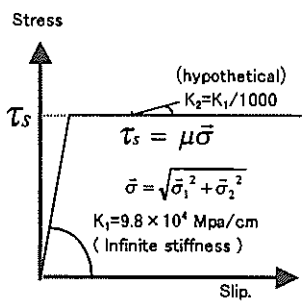

(1) x- directions

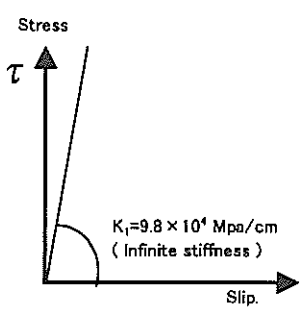

(2) y-,z- directions

Fig. 2 Stress-slip. relationships of friction model

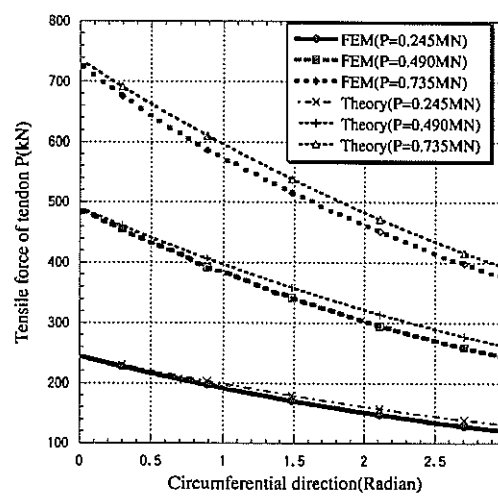

Fig. 4 Comparison of force distributions (μ =0. 21)

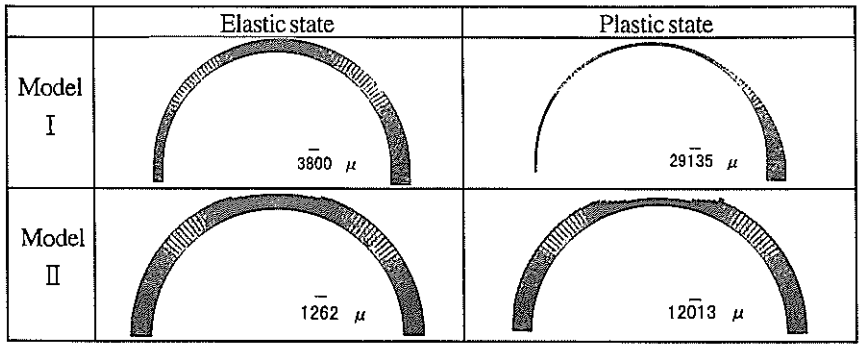

Fig.5 Strain distributon of the tendon

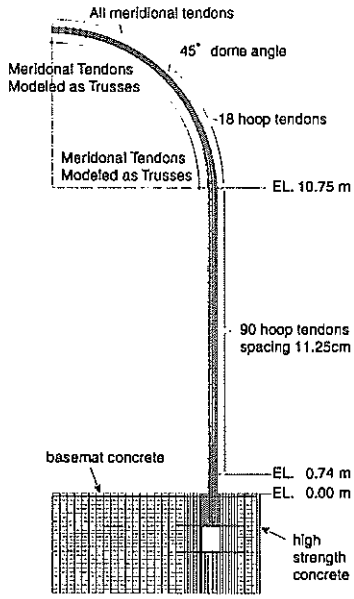

Fig.6 Computational grids (Axisymmetric model)

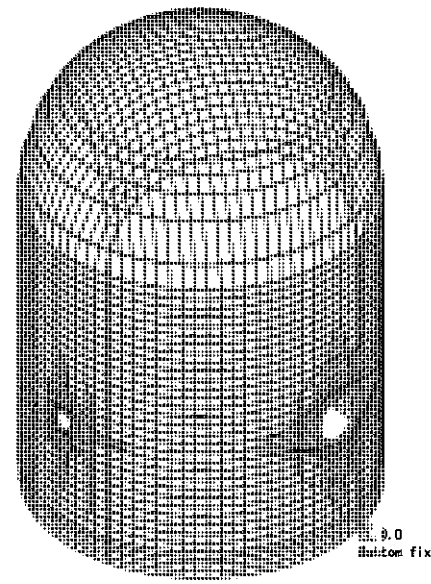

Fig.7 Computational grids (360° model)

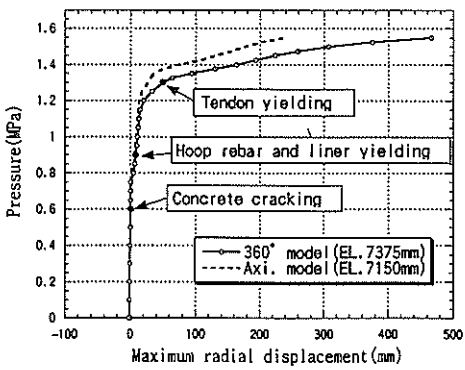

Fig.8 Pressure-radial displacement relationships at maximum displacement points

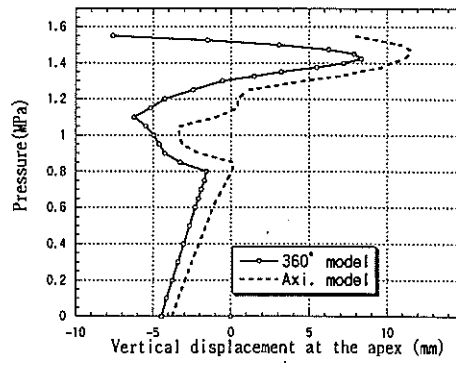

Fig.9 Pressure-vertical displacement relationships at apex of the dome

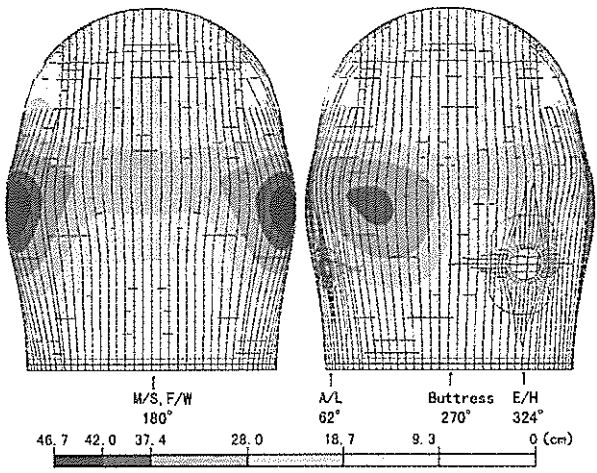

Fig.10 Deformation mode and contour

Table.1 Maximum strains versus pressure

		Pressure(MPa)		
		1.40	1.45	1.55
Tendon	Strain(%)	2.71	3.58	7.50
	Location	T1	T2	T3
Rebar	Strain(%)	3.68	5.06	9.21
	Location	R1	R2	R3
Liner	Strain(%)	3.79	9.21	9.29
	Location	L1	L2	L3

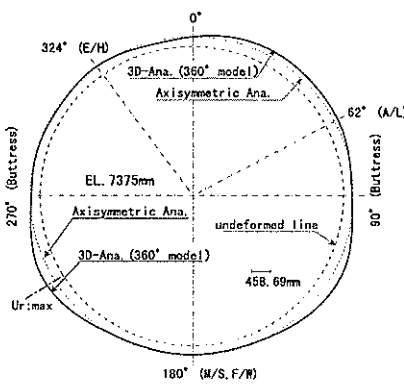

Fig.11 Radial displacement modes at the height of EL 7375

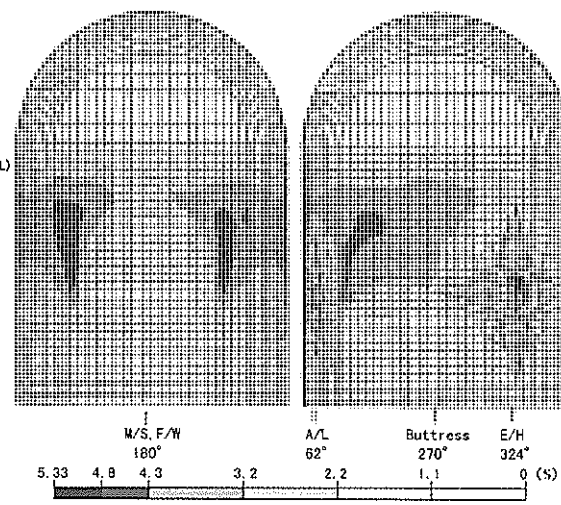

Fig.12 Contour of von Mises strain of liner

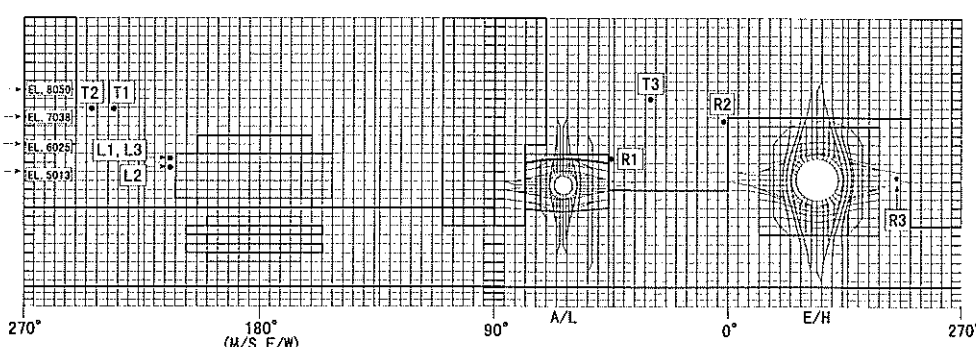

The marks (T1,R1,L1,etc) coreespond to the Table.1

Fig.13 Locations of the maximum strains of materials and rebar cut-off sections.